

On the environmental influence of groups and clusters of galaxies beyond the virial radius: Galactic conformity at few Mpc scales

Ivan Lacerna,^{1,2*} Facundo Rodriguez,^{3,4} Antonio D. Montero-Dorta,⁵
 Ana L. O’Mill,^{3,4} Sofía A. Cora,^{6,7} M. Celeste Artale,^{8,9} Andrés N. Ruiz,^{3,4}
 Tomás Hough⁶ and Cristian A. Vega-Martínez^{10,11}

¹ *Instituto de Astronomía y Ciencias Planetarias, Universidad de Atacama, Copayapu 485, Copiapó, Chile*

² *Millennium Institute of Astrophysics, Nuncio Monsenor Sotero Sanz 100, Of. 104, Providencia, Santiago, Chile*

³ *Instituto de Astronomía Teórica y Experimental, CONICET-UNC, Laprida 854, X5000BGR, Córdoba, Argentina*

⁴ *Observatorio Astronómico de Córdoba, UNC, Laprida 854, X5000BGR, Córdoba, Argentina.*

⁵ *Departamento de Física, Universidad Técnica Federico Santa María, Casilla 110-V, Avda. España 1680, Valparaíso, Chile*

⁶ *Instituto de Astrofísica de La Plata (CCT La Plata, CONICET, UNLP), Observatorio Astronómico, Paseo del Bosque B1900FWA, La Plata, Argentina*

⁷ *Facultad de Ciencias Astronómicas y Geofísicas, Universidad Nacional de La Plata, Observatorio Astronómico, Paseo del Bosque, B1900FWA La Plata, Argentina*

⁸ *Institut für Astro- und Teilchenphysik, Universität Innsbruck, Technikerstraße 25/8, A-6020 Innsbruck, Austria*

⁹ *Department of Physics and Astronomy, Purdue University, 525 Northwestern Avenue, West Lafayette, IN 47907, USA*

¹⁰ *Instituto de Investigación Multidisciplinar en Ciencia y Tecnología, Universidad de La Serena, Raúl Bitrán 1305, La Serena, Chile*

¹¹ *Departamento de Astronomía, Universidad de La Serena, Av. Juan Cisternas 1200 Norte, La Serena, Chile*

13 April 2022

ABSTRACT

The environment within dark matter haloes can quench the star formation of galaxies. However, environmental effects beyond the virial radius of haloes ($\gtrsim 1$ Mpc) are less evident. An example is the debated correlation between colour or star formation in central galaxies and neighbour galaxies in adjacent haloes at large separations of several Mpc, referred to as two-halo galactic conformity. We use two galaxy catalogues generated from different versions of the semi-analytic model SAG applied to the MDPL2 cosmological simulation and the ILLUSTRISTNG300 cosmological hydrodynamical simulation to study the two-halo conformity by measuring the quenched fraction of neighbouring galaxies as a function of the real-space distance from central galaxies. We find that low-mass central galaxies in the vicinity of massive systems ($M_{200c} \geq 10^{13} h^{-1} M_{\odot}$) out to $5 h^{-1}$ Mpc are preferentially quenched compared to other central galaxies at fixed stellar mass M_{\star} or fixed host halo mass M_{200c} at $z \sim 0$. In all the galaxy catalogues is consistent that the low-mass ($M_{\star} < 10^{10} h^{-1} M_{\odot}$ or $M_{200c} < 10^{11.8} h^{-1} M_{\odot}$) central galaxies in the vicinity of clusters and, especially, groups of galaxies mostly produce the two-halo galactic conformity. On average, the quenched low-mass central galaxies are much closer to massive haloes than star-forming central galaxies of the same mass (by a factor of ~ 5). Our results agree with other works regarding the environmental influence of massive haloes that can extend beyond the virial radius and affect nearby low-mass central galaxies.

Key words: galaxies: general – galaxies: haloes – galaxies: star formation – galaxies: groups: general – galaxies: clusters: general – galaxies: statistics

1 INTRODUCTION

The description of the dependence of the physical properties of galaxies on their environment is paramount to understand

* E-mail: ivan.lacerna@uda.cl

galaxy formation. Galaxies residing within groups and clusters are strongly affected by different processes that modify their gas content, e.g., ram-pressure stripping (Gunn & Gott 1972; Giovanelli & Haynes 1985; Aragon-Salamanca et al. 1993; Solanes et al. 2001; McCarthy et al. 2008; Cortese et al. 2011; Gavazzi et al. 2018; Lin et al. 2019; Roberts et al. 2019; Schaefer et al. 2019), starvation or ‘strangulation’ (Larson, Tinsley & Caldwell 1980; Peng, Maiolino & Cochrane 2015; Spindler et al. 2018; Garling et al. 2020), and high-speed galaxy encounters or ‘galaxy harassment’ (Moore et al. 1996; Moore, Lake & Katz 1998; Lin et al. 2010).

Interest in environmental effects at large scales ($\gtrsim 1$ Mpc), typically well beyond the virial radius of galaxy groups and clusters, has increased in the last few years (e.g., Wetzel, Tinker & Conroy 2012; Bahé et al. 2013; Benítez-Llambay et al. 2013; Cybulski et al. 2014; Campbell et al. 2015; Hearin, Watson & van den Bosch 2015; Bahé et al. 2017; Goddard et al. 2017; Zheng et al. 2017; Zinger et al. 2018; Duckworth et al. 2019; Kraljic et al. 2019; Pallero et al. 2019; Tremmel et al. 2019; Zheng et al. 2019; Pandey & Sarkar 2020; Zhang, Yang & Guo 2021). The effect of the large-scale environment on massive galaxies is less strong than the effect of mass (e.g. Alpaslan et al. 2015), but seems to play a role in less massive galaxies (Peng et al. 2010; Bluck et al. 2014; Argudo-Fernández, Lacerna & Duarte Puertas 2018). The minimum role of the large-scale environment at higher masses is likely due to the dominant presence of active galactic nuclei (AGN) feedback in these galaxies (e.g. Bower et al. 2006; Hirschmann et al. 2013; Bluck et al. 2016; Guo et al. 2019). Environmental effects also depend on the orbital evolution of galaxies. Galaxies found beyond the virial radius of the cluster (1–2 Mpc from the cluster centre) might be recent infallers or galaxies that have passed once near the cluster centre, where environmental effects are stronger and are in their way out of the cluster. Galaxies that experienced this latter phenomenon are known as “backsplash” galaxies (Gill, Knebe & Gibson 2005; Pimblet 2011; Muriel & Coenda 2014; Haggard et al. 2020). About 60 per cent of galaxies in the region between one and two virial radii around a galaxy cluster would be backsplash galaxies (Haggard et al. 2020).

A remarkable case of the effect of the environment at different scales is galactic conformity (e.g. Weinmann et al. 2006; Kauffmann et al. 2013; Phillips et al. 2014; Kauffmann 2015; Knobel et al. 2015; Paranjape et al. 2015; Bray et al. 2016; Hearin, Behroozi & van den Bosch 2016; Lee et al. 2016; Berti et al. 2017; Sin, Lilly & Henriques 2017; Calderon, Berlind & Sinha 2018; Lacerna et al. 2018; Rafieferantsoa & Davé 2018; Sun et al. 2018; Tinker et al. 2018; Treyer et al. 2018; Zu & Mandelbaum 2018; Sin, Lilly & Henriques 2019; Alam et al. 2020; Otter et al. 2020; Li et al. 2021; Maier, Haines & Ziegler 2022). This term is used to describe the observed correlation between colour or star formation activity in central galaxies and their satellite galaxies. Observationally, central galaxies are usually identified in the centre of galaxy groups or clusters or as galaxies without relatively bright neighbours; theoretically, they reside near the centre of the potential well of host dark matter haloes. Weinmann et al. (2006) defined the term galactic conformity after finding that quenched central galaxies have a higher fraction of quenched satellite galaxies compared to star-forming central galaxies in galaxy groups of similar

mass at $z < 0.05$. Later, Kauffmann et al. (2013) found a galactic conformity effect between low-mass central galaxies with low specific star formation rate (sSFR) or gas content and neighbour galaxies with low sSFR out to scales of 4 Mpc at $z < 0.03$. These results motivated the distinction between the conformity measured at small separations between the central galaxy and their satellite galaxies within a dark matter halo and the signal measured at large separations of several Mpc between the central galaxy and neighbour galaxies in adjacent haloes. The former is referred to as one-halo conformity, while the latter is called two-halo conformity.

Cosmological hydrodynamical simulations (e.g. Bray et al. 2016), semi-analytic models of galaxy formation (e.g. Lacerna et al. 2018), and mock galaxy catalogues (e.g. Sin, Lilly & Henriques 2017; Tinker et al. 2018) show a correlation in colour or star formation between central (primary) galaxies and neighbour (secondary) galaxies at Mpc scales, i.e., two-halo conformity. However, the signal is smaller compared to observations because the latter use isolation criteria to select primary galaxies that include a small fraction of satellite galaxies. The overall two-halo conformity decreases when only central galaxies are considered in the selection of the primaries (Bray et al. 2016; Sin, Lilly & Henriques 2017; Lacerna et al. 2018; Tinker et al. 2018). Furthermore, Sin, Lilly & Henriques (2017) found that the two-halo conformity out to projected distances of 3–4 Mpc from central galaxies in mock catalogues is primarily related to the environmental influence of very large neighbouring haloes. Zinger et al. (2018) suggest that the scenario of satellite quenching in the environment of galaxy clusters, which extends to ~ 2 – 3 virial radii, is consistent with the galactic conformity over large distance scales of several Mpc. On the other hand, Lacerna et al. (2018) found that the two-halo conformity is only detected for central galaxies in relatively low-mass haloes ($M_{\text{halo}} \leq 10^{12.4} h^{-1}$ Mpc). It has been shown that relatively massive haloes could disrupt the average growth of near smaller objects (e.g. Wang, Mo & Jing 2007; Dalal et al. 2008; Hahn et al. 2009; Behroozi et al. 2014) and, therefore, affect their properties (e.g. Lacerna & Padilla 2011; Salcedo et al. 2018; Mansfield & Kravtsov 2020). Thus, the two-halo conformity may result from galaxies hosted by low-mass haloes affected by nearby massive systems.

This paper uses cosmological numerical simulations to extend previous works about galaxies that are quenched preferentially in the infall region around dense and massive structures in the local Universe. In particular, we study whether the two-halo conformity at a few Mpc scales is given by central galaxies in the vicinity of galaxy groups and clusters.

The outline of the paper is as follows. Section 2 describes the cosmological simulations and synthetic galaxy catalogues used in this paper. The methodology to measure galactic conformity is presented in Section 3. The results with the correlations of sSFR are shown in Section 4. We discuss our results in Section 5 and the conclusions are given in Section 6.

The cosmological simulations in this paper use different values of the reduced Hubble constant, h , defined as $H_0 = 100 h \text{ km s}^{-1} \text{ Mpc}^{-1}$. We opted for scaling h explicitly throughout this paper with the following dependencies

unless the value of h is specified: stellar mass and halo mass in $h^{-1} M_{\odot}$, physical scale in h^{-1} Mpc, and sSFR in $h \text{ yr}^{-1}$.

2 COSMOLOGICAL SIMULATIONS

We use cosmological numerical simulations of big volumes that contain a large number of galaxy groups and clusters to obtain statistically significant results, and with a good mass resolution to sample galaxies with stellar masses above $7 \times 10^8 h^{-1} M_{\odot}$ as well. We study the conformity at few Mpc scales using three different galaxy catalogues: two generated by applying a semi-analytic model (SAM) of galaxy formation and evolution to a large N -body simulation of dark matter (Sect. 2.1), and other extracted from a cosmological hydrodynamical simulation (Sect. 2.2).

It is worth noticing that the scope of this paper is not to compare results from SAMs and hydrodynamical simulations, but to study a possible excess of correlation in star formation and colour out to scales of few Mpc as a result of the presence of central galaxies in the vicinity of relatively massive systems using different types of galaxy formation models. In this regard, this paper does not have a simulated fiducial catalogue.

2.1 SAG galaxy catalogues

We analyse two galaxy catalogues generated by applying the SAM SAG to the dark matter only MultiDark Planck 2 (MDPL2) cosmological simulation (Klypin et al. 2016; Knebe et al. 2018). The model SAG originates from the SAM described in Springel et al. (2001b) and was subsequently modified as detailed in Cora (2006), Lagos, Cora & Padilla (2008), Tecce et al. (2010), Orsi et al. (2014), Muñoz Arancibia et al. (2015), Gargiulo et al. (2015) and Cora et al. (2018); the latter work presents the latest version of the model. The MDPL2 has a huge volume of $(1 h^{-1} \text{ Gpc})^3$ and dark matter mass resolution of $1.5 \times 10^9 h^{-1} M_{\odot}$. It is consistent with a flat Λ CDM model characterized by Planck cosmological parameters: $\Omega_m = 0.307$, $\Omega_{\Lambda} = 0.693$, $\Omega_B = 0.048$, $n_s = 0.96$ and $H_0 = 100 h^{-1} \text{ km s}^{-1} \text{ Mpc}^{-1}$, where $h = 0.678$ (Planck Collaboration et al. 2014). Dark matter haloes have been identified with the ROCKSTAR halo finder (Behroozi, Wechsler & Wu 2013), and merger trees were constructed with CONSISTENTTREES (Behroozi et al. 2013).

The halo catalogues and merger trees constitute the input of the model SAG which assigns one galaxy to each new detected halo in the simulation to generate the galaxy population. Central galaxies reside within main host haloes detected over the background density. Those haloes lying within another dark matter halo are subhaloes and contain satellite galaxies. Those galaxies that are assigned to dark matter subhaloes that are no longer identified by the halo finder (either because they have been disrupted by tidal effects or merged with the main host halo, or simply because of resolution effects of the underlying simulation) are called orphan satellites, and their orbital evolution is tracked semi-analytically in a pre-processing step before applying SAG to

the dark matter only simulation (Cora et al. 2018; Delfino et al. 2022).¹

The evolution of galaxy properties is tracked by SAG considering a set of physical processes that regulate the circulation of mass and metals among the different baryonic components of the galaxy (hot gas halo, gaseous and stellar discs, stellar bulge), namely, radiative cooling of the hot halo gas, star formation (quiescent and in starbursts triggered by mergers and disc instabilities), chemical enrichment produced by stellar winds and different types of supernovae, feedback from supernovae and from active galactic nuclei, and environmental effects such as tidal stripping and ram pressure stripping. In particular, the value of ram pressure at the radial position of the satellite galaxies is obtained from an analytic profile that depends on halo mass and redshift, obtained by fitting the information provided by hydrodynamical simulations of groups and clusters of galaxies (Vega-Martínez et al. 2022). Ram pressure exerted over satellite galaxies removes their hot gas gradually after infall. When the ratio between the hot gas mass and the baryonic mass of a satellite decreases below 0.1, ram pressure can strip gas from the galaxy disc. The implementations of all these processes involve free parameters that have been calibrated to a set of observed relations of galaxy properties by using the *Particle Swarm Optimisation* technique (Ruiz et al. 2015).

The two galaxy catalogues used in this study have been generated with the version of SAG previously described, and differ only in the value of the parameter β involved in the explicit redshift dependence of the reheated and ejected mass by supernovae feedback (see equation 10 and 12 of Cora et al. 2018), which is based on relations measured from full-physics hydrodynamical simulations. One of the catalogues is characterized by a value given by the calibration process ($\beta = 1.99$), while the other was generated by adopting a smaller value ($\beta = 1.3$) in order to achieve better consistency with the observational trends followed by the fraction of local passive satellites as a function of stellar mass, halo mass, and the halo-centric distances (Cora et al. 2018). However, the larger value of β allows to reproduce the evolution of the mass-metallicity relation of galaxies in the redshift range $0 < z < 3.5$ (Collacchioni et al. 2018). We refer to the galaxy catalogues with the larger and smaller values of β as MD_SAG and SAG $_{\beta 1.3}$, respectively.

The MD_SAG galaxy catalogue contains about 370,000 galaxy groups and clusters with $M_{200c} \geq 10^{13} h^{-1} M_{\odot}$, where M_{200c} is the dark matter halo mass within a radius that contains a mean density of 200 times the critical density of the Universe, and about 40 million galaxies with stellar mass above $7 \times 10^8 h^{-1} M_{\odot}$. This catalogue includes relevant physical parameters such as the stellar mass, SFR, *ugriz* magnitudes, bulge-to-total stellar mass ratio, and the distinction between central and satellite galaxies. The sSFR and $g-r$ colour distributions as functions of the stellar mass are shown in the left column of Fig. 1 for all galaxies (cen-

¹ The orbital evolution model described in Delfino et al. (2022) considers a NFW density profile (Navarro, Frenk & White 1997) for both the host halo and the unresolved subhalo. Here, a previous version of the model is used assuming an isothermal density profile for both cases.

trals and satellites) in the MD_SAG catalogue. Similar distributions are obtained for the galaxies in the SAG $_{\beta 1.3}$ catalogue (not shown). Although the fraction of quenched galaxies is in better agreement with observational measurements in the latter case, as already mentioned, we decided to show the results of our analysis for both the MD_SAG and SAG $_{\beta 1.3}$ catalogues since the former is publicly available² (Knebe et al. 2018) and allows the reproducibility of our results.

2.2 The ILLUSTRISTNG300 hydrodynamical simulation

Cosmological hydrodynamical simulations have the benefit of providing predictions that are less model-dependent than those coming from SAMs, because they follow the evolution of dark matter particles, gas cells, and stellar particles simultaneously in a self-consistent way. Therefore, we also use the ILLUSTRISTNG simulation (Naiman et al. 2018; Nelson et al. 2018; Marinacci et al. 2018; Pillepich et al. 2018b; Springel et al. 2018; Nelson et al. 2019). Among the different boxes, we choose ILLUSTRISTNG300, which is one of the largest magneto-hydrodynamical cosmological simulations available, with a side length of $205 h^{-1}$ Mpc. The ILLUSTRISTNG300 simulation adopts the standard Λ CDM cosmology (Planck Collaboration et al. 2016), with parameters $\Omega_m = 0.3089$, $\Omega_b = 0.0486$, $\Omega_\Lambda = 0.6911$, $H_0 = 100 h \text{ km s}^{-1} \text{ Mpc}^{-1}$ with $h = 0.6774$, $\sigma_8 = 0.8159$, and $n_s = 0.9667$. It follows the evolution of 2500^3 dark-matter particles of mass $4.0 \times 10^7 h^{-1} M_\odot$, and 2500^3 gas cells with a mass of $7.6 \times 10^6 h^{-1} M_\odot$. ILLUSTRISTNG300 contains about 4000 galaxy groups and galaxy clusters with masses between $10^{13} \leq M_{200c}/M_\odot \leq 10^{15}$, and 280 galaxy clusters with $M_{200c} > 10^{14} M_\odot$ (Pillepich et al. 2018a).

The ILLUSTRISTNG simulation suite was built using the AREPO moving-mesh code (Springel 2010) and is regarded as an improved version of its predecessor, the ILLUSTRIS simulation (Vogelsberger et al. 2014b,a; Genel et al. 2014). Its updated sub-grid models account for a variety of physical processes, including star formation, radiative metal cooling, chemical enrichment from Type II and Type Ia supernovae (SNe) events, and asymptotic giant branch (AGB) stars, stellar feedback, and super-massive black hole feedback (see Weinberger et al. 2017; Pillepich et al. 2018b, for more details). Importantly, these models were specifically calibrated to reproduce important observational constraints such as the observed $z = 0$ galaxy stellar mass function,³ the cosmic SFR density, the halo gas fraction, the galaxy stellar size distributions, or the black hole – galaxy mass relation.

As for dark matter haloes, these objects are defined in ILLUSTRISTNG using a friends-of-friends (FOF) algorithm with a linking length of 0.2 times the mean inter-particle separation (Davis et al. 1985). The gravitationally bound substructures that we call subhaloes are, in turn, identified using the SUBFIND algorithm (Springel et al. 2001a; Dolag

et al. 2009). In IllustrisTNG, all subhaloes containing a non-zero stellar mass component are labelled galaxies, but here we use a stellar-mass threshold of $10^9 h^{-1} M_\odot$ (see Sec. 3).

The IllustrisTNG simulation has been an excellent tool for studying the connection between galaxies and dark matter haloes at small and large scales. Among others, it has been implemented to study the occupancy variations (Bose et al. 2019; Hadzhiyska et al. 2020), the impact of secondary halo properties on the galaxy population (Montero-Dorta et al. 2020; Contreras, Angulo & Zennaro 2021; Montero-Dorta et al. 2021; Favole et al. 2022), and the galaxy size relation of satellite and central galaxies with their host dark matter haloes (Rodríguez et al. 2021). The distributions of the sSFR and $g - r$ colour as functions of the stellar mass in the IllustrisTNG300 simulation are shown in the right panels of Fig. 1.

3 METHODOLOGY

There are different ways to measure correlations of galaxy properties between central and neighbouring galaxies. For example, Kauffmann et al. (2013) measured the sSFR of neighbouring galaxies around isolated galaxies, as observational proxies of central galaxies, as a function of the projected distance from the central galaxies at a given stellar mass bin. This approach has also been used in mock catalogues (e.g. Sin, Lilly & Henriques 2017; Tinker et al. 2018). Another approach is to estimate the mean red fraction or mean quenched fraction of neighbouring (secondary) galaxies as a function of the distance from the central (primary) galaxies in stellar mass bins of the centrals. In simulations, the distance is estimated in real space (e.g. Bray et al. 2016; Lacerna et al. 2018). Here, we use the latter approach because the comparison with observations is outside the scope of the current paper. This aspect will be a matter of another work. Instead, we focus on the results obtained directly from the boxes of the simulations at $z \sim 0$. In this way, we can assess the results under ideal conditions in the simulations.

Galaxies with stellar mass $M_* > 7 \times 10^8 h^{-1} M_\odot$ in the samples built from the SAG model and $M_* > 10^9 h^{-1} M_\odot$ from the ILLUSTRISTNG300 simulation are classified according to sSFR, $g - r$ colour, stellar mass bins, and halo mass (M_{200c}) bins. Synthetic galaxies are well modelled down to these thresholds in stellar mass in these catalogues. For instance, the low-mass end of the observed stellar mass function at $z \sim 0$ is well reproduced until this lower limit in the SAG model (see fig. 1 of Cora et al. 2018). For ILLUSTRISTNG300, the lower limit in stellar mass corresponds to approximately 130 gas cells. This threshold is consistent with previous works (e.g. Pillepich et al. 2018a; Donnari et al. 2019; Montero-Dorta et al. 2020; Donnari et al. 2021). Furthermore, there is an overall good agreement in these galaxy catalogues with the observed quenched fraction of low-mass central galaxies at low redshift (e.g. see Xie et al. 2020; Donnari et al. 2021). Although these galaxy catalogues tend to overestimate the fraction of low-mass quenched satellite galaxies in low-mass haloes (Cora et al. 2018; Xie et al. 2020; Donnari et al. 2021), these quenched fractions in simulations reduce when similar conditions to the observations are applied (Donnari et al. 2021).

By establishing a cut or threshold in sSFR and colour,

² The catalogue is accessible from the CosmoSim database <http://www.cosmosim.org/>

³ Note that we have used the standard ILLUSTRISTNG300 galaxy catalogue. The best agreement between the model and the observational data, as far as the stellar content of haloes is concerned, is obtained with a modified catalogue where stellar masses are slightly re-scaled (see Pillepich et al. 2018a for more information).

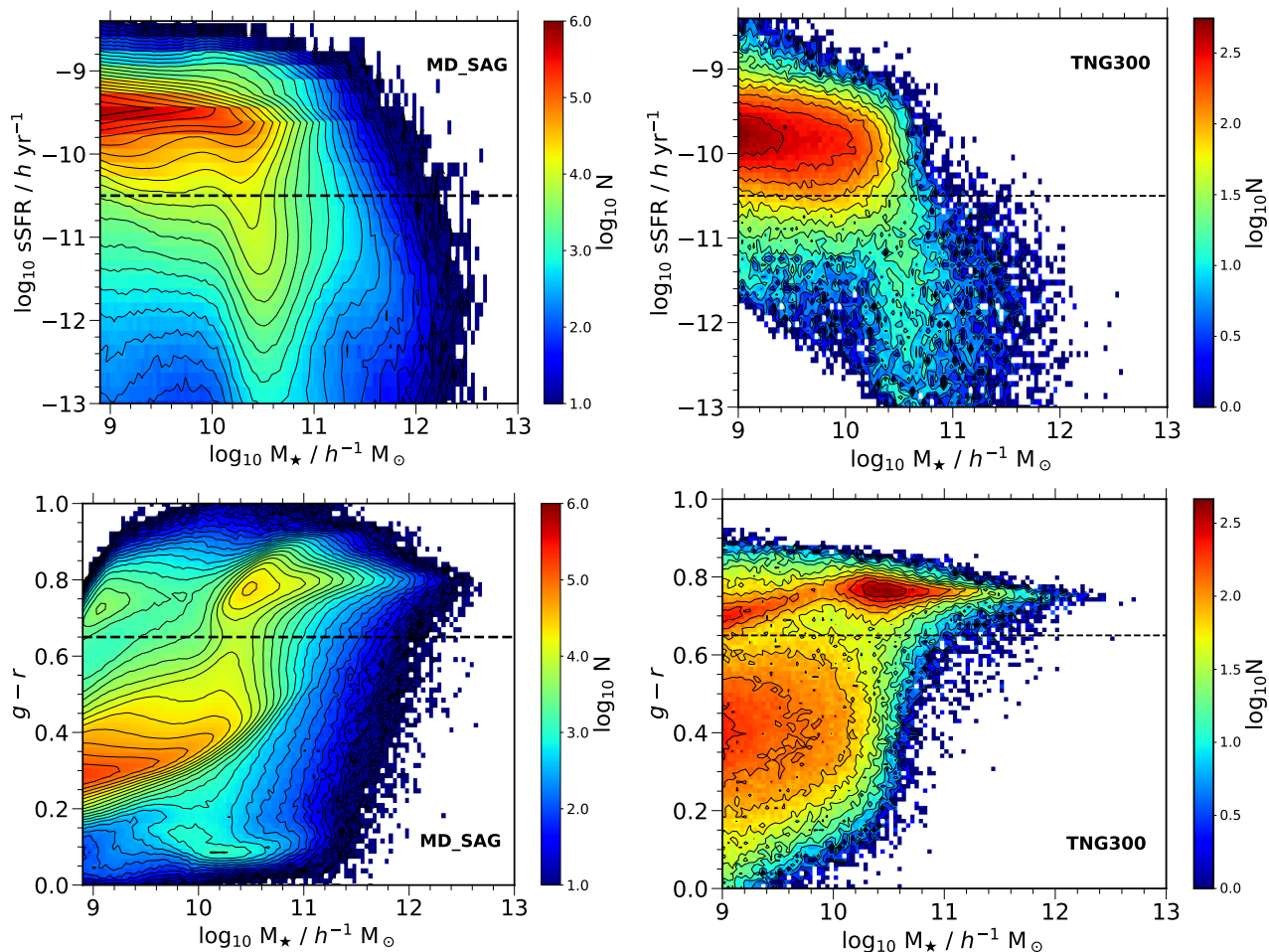


Figure 1. Distributions of sSFR (top panels) and $g-r$ colour (bottom panels) as functions of the stellar mass for synthetic galaxies (centrals and satellites) in the MD_SAG catalogue (left) and ILLUSTRISTNG300 simulation (right), represented by contours coloured-coded according to the number density of galaxies, as indicated in the colour bars. The black dashed lines depict the fiducial values that roughly separates quenched and star-forming galaxies (top) and red and blue galaxies (bottom).

we can select the galaxies with quenched star formation and red colours. We refer to a galaxy as quenched if the $\text{sSFR} \leq 10^{-10.5} h \text{ yr}^{-1}$, whereas galaxies with sSFR above this value are considered as star-forming galaxies (e.g., see the dashed line in the top panels of Fig. 1). The chosen value in sSFR is based on Brown et al. (2017) for selecting star-forming galaxies. Cora et al. (2018) found that this cut in sSFR ($10^{-10.7} \text{ yr}^{-1}$ with $h = 0.678$) allows a better separation between star-forming and quiescent galaxies in the SAG model than other cuts commonly used in the literature, e.g. $\text{sSFR} = 10^{-11} \text{ yr}^{-1}$ (Wetzel, Tinker & Conroy 2012). We opted for using the same cut in sSFR for the ILLUSTRISTNG300 galaxy catalogue for consistency, avoiding biased results for particular cuts in each catalogue. We obtain a fraction of quenched galaxies of 14 per cent for the MD_SAG galaxy catalogue, 17 per cent for the SAG $_{\beta 1.3}$ one, and 38 per cent for the ILLUSTRISTNG300 simulation. Although the fraction of quenched galaxies is smaller in the SAG galaxy catalogues compared to the ILLUSTRISTNG300 one, the top panels of Fig. 1 show that both MD_SAG and ILLUSTRISTNG300 models have a similar concentration of star-forming galaxies using this cut in sSFR.

Likewise, we refer to a galaxy as red if $g-r \geq 0.65$, whereas galaxies with colours below this value are considered blue galaxies (e.g. see the dashed line in the bottom panels of Fig. 1). We selected this colour cut from the bimodality in the MD_SAG galaxy catalogue (bottom left panel in Fig. 1). The chosen value is in rough agreement with the separation between the red sequence and the blue cloud in the Sloan Digital Sky Survey (SDSS) galaxies (e.g. Blanton & Moustakas 2009). We obtain a fraction of red galaxies of 12 per cent for the MD_SAG catalogue. Again, we opted to use the same colour cut for the other galaxy catalogues for consistency. The fraction of red galaxies is 15 per cent for SAG $_{\beta 1.3}$ and 31 per cent for ILLUSTRISTNG300 catalogues. Although the fractions of red galaxies are different between the SAG galaxy catalogues and the ILLUSTRISTNG300 one, their colour distributions are similar, in general. They show a blue cloud and the red sequence, separated by the chosen colour cut.

With the distinction of central and satellite galaxies as defined by the corresponding halo finders of each available catalogue, we can measure the mean quenched fraction f_Q or the mean red fraction f_r of neighbouring (secondary) galax-

ies around central (primary) galaxies at fixed mass to assess the galactic conformity. The neighbouring galaxies are all the galaxies (centrals and satellites) above the M_* threshold out to a real-space distance of $10 h^{-1}$ Mpc from the central galaxies in each sample of primary galaxies. To measure the galactic conformity at a given distance, we estimate the mean fractions of quenched (red) neighbouring galaxies around both quenched (red) and star-forming (blue) primary galaxies at fixed stellar or halo mass,⁴ and calculate the difference between these fractions, Δf_Q (Δf_r). If the difference is close to zero, there is no correlation between the sSFR or colour of central galaxies and their neighbouring galaxies, i.e., there is no conformity. Therefore, galactic conformity becomes more prominent as the difference, Δf_Q , increases. Although our galaxy catalogues are imperfect in reproducing all the observed trends regarding the absolute quenched fractions, these discrepancies do not significantly affect the differences in the quenched fractions at fixed mass, i.e., the galactic conformity signal.

We will refer to the primary sample with *all* the central galaxies at fixed mass as ‘PrimAll’. The conformity signal with the ‘PrimAll’ sample is the fiducial case of two-halo conformity measured in simulations and observations. We then repeat the same procedure, but removing central galaxies in the vicinity around massive systems of $M_{200c} \geq 10^{13} h^{-1} M_\odot$ out to $5 h^{-1}$ Mpc. We choose this scale as a simple representation of the large-scale environment beyond the virial radius of host haloes (e.g. Argudo-Fernández, Lacerna & Duarte Puertas 2018), which is also a scale that is typically larger than filament thickness (Kuutma, Tamm & Tempel 2017). We discuss the chosen vicinity radius in Sec. 5.2. The central galaxies within the vicinity radius around massive systems are only removed from the primary sample. The secondary sample of neighbouring galaxies out to $10 h^{-1}$ Mpc of each remaining primary galaxy is the same. We will refer to this primary sample that does not include central galaxies around clusters (AC) or groups as ‘PrimNotAC’.

The analysis of samples ‘PrimAll’ and ‘PrimNotAC’ will allow us to establish the contribution of central galaxies located around massive systems on the two-halo conformity signal measured at separations of several Mpc. An excess of conformity signal at few Mpc scales by considering *all* the central galaxies in ‘PrimAll’ with respect to the signal corresponding to the case ‘PrimNotAC’ will confirm that the two-halo conformity, i.e., correlations of star formation or colour between central galaxies and neighbouring galaxies beyond the virial radius of virialized structures, can be explained mainly by the presence of central galaxies in the outskirts of rich galaxy groups and clusters.

The errors in the estimation of the mean fractions for the SAG catalogues are calculated using the jackknife method (e.g. Zehavi et al. 2002; Norberg et al. 2009). For this, we split every sample into 120 subsamples. Error bars in the

⁴ We will estimate the mean fractions of neighbouring galaxies for separations between $0.6 h^{-1}$ Mpc out to $10 h^{-1}$ Mpc from the primary galaxies, but we will discuss the results for scales $r \gtrsim 1 h^{-1}$ Mpc because we are interested in the two-halo conformity. At smaller scales, the conformity signal might be mixed with that from the one-halo conformity.

mean fractions are estimated using the diagonal of the covariance matrix. Given the large number of galaxies, the error bars are small enough to be imperceptible in some of the following figures.

The methodology for estimating errors is slightly different for ILLUSTRISTNG300, but it is also based on a jackknife technique. The box is divided in 8 subboxes ($L_{\text{sub-box}} = L_{\text{box}}/2 = 102.5 h^{-1}\text{Mpc}$) so that one subbox at a time is disregarded. The uncertainties on the mean fractions correspond to the standard deviation computed from the 8 subvolumes ($V_i = \frac{7}{8} V_{\text{total}}$).

4 RESULTS

Figure 2 shows the mean quenched fractions of neighbouring galaxies as functions of the distance from the primary galaxies in two stellar-mass bins in the MD_SAG catalogue.⁵ The solid lines correspond to *all* the central galaxies in the primary sample, ‘PrimAll’. The mean quenched fraction (f_Q) is higher around quenched central galaxies (dark red solid line) compared with that around star-forming centrals (navy blue solid line) up to $3 h^{-1}$ Mpc from low-mass central galaxies (top panels). Both fractions tend to converge to the overall quenched fraction of this galaxy catalogue at large scales of about $10 h^{-1}$ Mpc. The sub-panels of Fig. 2 show the difference between both mean quenched fractions (Δf_Q) as a function of the distance from the central galaxies for the same stellar mass bins (solid lines). The difference is as big as $\Delta f_Q \sim 0.15$ at $\sim 1 h^{-1}$ Mpc for low-mass primary galaxies of $10^{9.7} \leq M_*/h^{-1} M_\odot < 10^{10}$, and declines to $\Delta f_Q \lesssim 0.05$ at distances $r \gtrsim 3 h^{-1}$ Mpc. For primary galaxies of $10^{10.3} \leq M_*/h^{-1} M_\odot < 10^{10.5}$, the difference in the quenched fractions of neighbours is always smaller than 0.02. This result confirms that the two-halo conformity is much stronger for low-mass central galaxies (e.g. Kauffmann et al. 2013; Bray et al. 2016; Lacerna et al. 2018).

For the sample ‘PrimNotAC’, in which the central galaxies in the vicinity of groups and clusters of galaxies are removed from the primary sample, the mean quenched fraction is slightly higher around quenched central galaxies compared with that around star-forming centrals (red and blue dashed lines in Fig. 2, respectively). The mean quenched fractions in ‘PrimNotAC’ increase to converge to the overall fraction of quenched galaxies of this catalogue from distances $\gtrsim 5 h^{-1}$ Mpc because of the spatial condition in which we remove the centrals in the vicinity of massive structures. The sub-panels of Fig. 2 show the differences in the quenched fractions (dashed line). These differences are much smaller than the case ‘PrimAll’ of the same stellar mass, with $\Delta f_Q \lesssim 0.02$ for scales $r \gtrsim 1 h^{-1}$ Mpc in both stellar mass bins. The excess of two-halo conformity at fixed stellar mass in ‘PrimAll’ compared with the case

⁵ We arbitrarily chose those stellar mass bins to remark results for low-mass central galaxies $M_* < 10^{10} h^{-1} M_\odot$ and for intermediate-mass central galaxies with $M_* \sim 10^{10.4} h^{-1} M_\odot$. We confirmed that the results for central galaxies between these two M_* bins correspond to a transition in the conformity signal shown in the two panels of Figure 2. The latter is also valid for the other galaxy catalogues used in this paper.

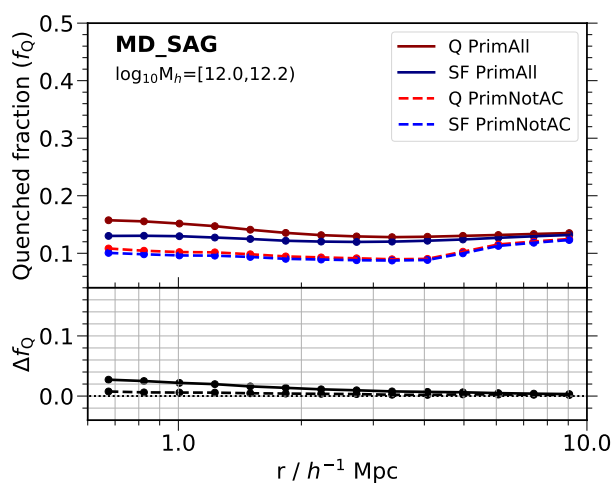
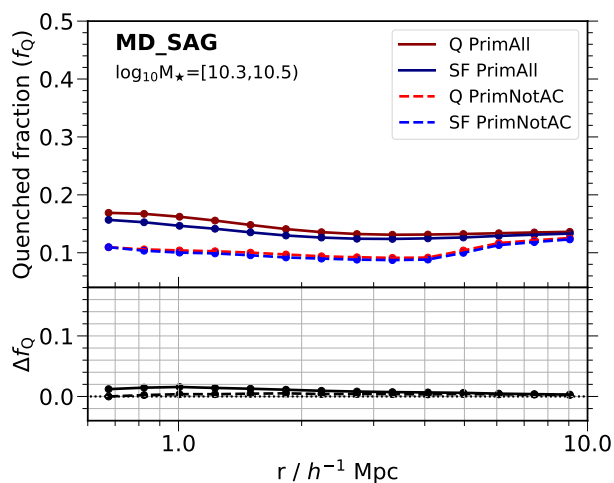
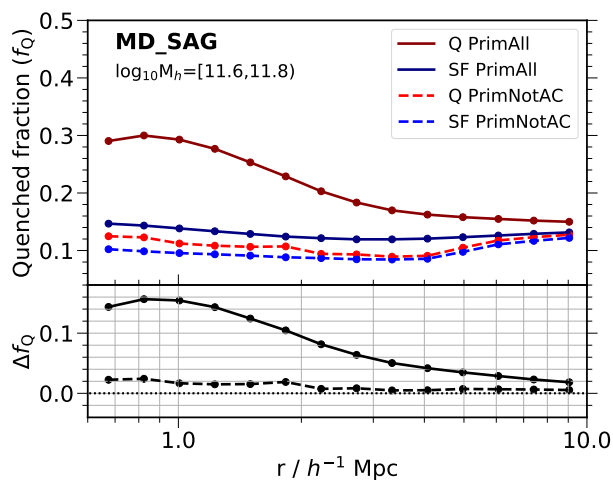
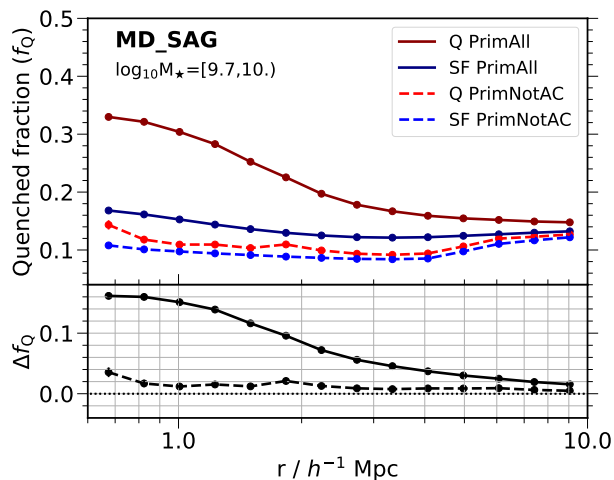


Figure 2. Main panels: mean quenched fractions of neighbouring galaxies as functions of the (real-space) distance from the primary galaxies in the MD_SAG catalogue. The primary galaxies are separated in two stellar-mass bins: $10^{9.7} \leq M_*/h^{-1} M_\odot < 10^{10}$ (top) and $10^{10.3} \leq M_*/h^{-1} M_\odot < 10^{10.5}$ (bottom). The solid lines consider all the central galaxies in the primary sample, ‘PrimAll’ (dark red and navy blue for quenched and star-forming primary galaxies). The dashed lines correspond to the mean fractions after removing the central galaxies in the vicinity of haloes more massive than $10^{13} h^{-1} M_\odot$ from the primary sample, case ‘PrimNotAC’ (red and blue for quenched and star-forming primary galaxies). Sub-panels: difference of the mean quenched fractions of neighbouring galaxies around quenched and star-forming primary galaxies at fixed stellar mass. The x-axis is the distance from the primary galaxies. The solid line shows the case ‘PrimAll’, whereas the dashed line is the result obtained for the case ‘PrimNotAC’. The dotted line denotes the case of zero difference, i.e. no conformity.

‘PrimNotAC’ supports the claim that most of the conformity signal at few Mpc scales can mainly be explained by the central galaxies in the outskirts of rich galaxy groups and clusters.

The results above assume that the correlations in sSFR between central and neighbouring galaxies are given by the stellar mass of the primary galaxies, as the resulting two-halo conformity is stronger for low-mass primary galaxies.

Figure 3. Same as Fig. 2 but for primary galaxies at fixed halo mass in the MD_SAG catalogue (from top to bottom: $10^{11.6} \leq M_{200c}/h^{-1} M_\odot < 10^{11.8}$ and $10^{12} \leq M_{200c}/h^{-1} M_\odot < 10^{12.2}$).

However, some authors (e.g. Paranjape et al. 2015; Tinker et al. 2018; Treyer et al. 2018) have suggested that the observed conformity at $\lesssim 4$ Mpc is because red (quenched) central galaxies can reside in more massive dark matter haloes than blue centrals of the same stellar mass. In this regard, for $M_* > 10^{10} h^{-1} M_\odot$, the median halo mass of quenched central galaxies is higher than that of star-forming central galaxies at fixed stellar mass (Lacerna et al. 2018). Fig. 3 shows the same exercise as before but for primary galaxies at fixed halo mass. We find qualitatively the same results as for primary galaxies at fixed stellar mass, i.e., there is an excess of correlation between quenched neighbouring galaxies and quenched primary galaxies out to several Mpc distances in the case ‘PrimAll’ (solid lines) compared with the case ‘PrimNotAC’ (dashed lines). The correlation is stronger for primary galaxies in lower mass haloes, but it is drastically reduced for the case in which the central galaxies in the vicinity of galaxy groups and clusters are removed from the primary sample at fixed halo mass. For instance, for primary galaxies at $10^{11.6} \leq M_{200c}/h^{-1} M_\odot < 10^{11.8}$, the difference of the mean quenched fractions of neighbours is $\Delta f_Q \sim 0.15$ (0.1) at $r \sim 1$ (2) h^{-1} Mpc from the primary galaxies in

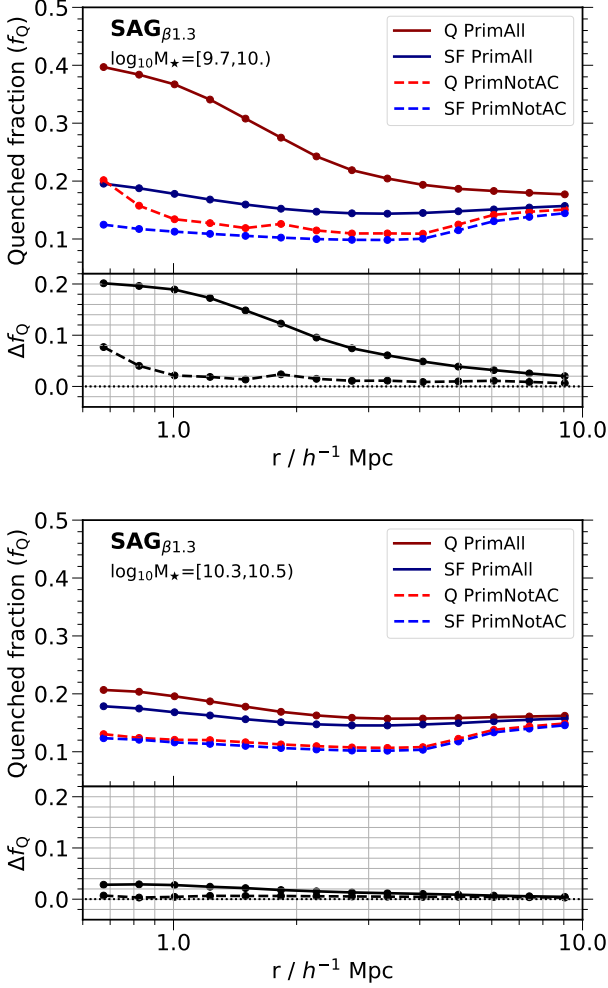


Figure 4. Same as Fig. 2 but for primary galaxies at fixed stellar mass in the $SAG_{\beta 1.3}$ galaxy catalogue.

the case ‘PrimAll’, but it is $\Delta f_Q \lesssim 0.02$ at scales $r \gtrsim 1 h^{-1}$ Mpc from primary galaxies in the case ‘PrimNotAC’ with the same host halo mass. For primary galaxies at intermediate halo masses ($10^{12} \leq M_{200c}/h^{-1} M_{\odot} < 10^{12.2}$, bottom panel), both cases ‘PrimAll’ and ‘PrimNotAC’ show $\Delta f_Q \lesssim 0.02$ at distances $r \gtrsim 1 h^{-1}$ Mpc. Therefore, the conformity measured at few Mpc scales is largely driven by low-mass central galaxies or central galaxies in low-mass haloes located in the outskirts of galaxy groups and galaxy clusters.

We now repeat the same test but using the $SAG_{\beta 1.3}$ galaxy catalogue. The results at fixed stellar mass for the primary galaxies are shown in Fig. 4. The trends are very similar to those obtained from the MD_SAG catalogue (Fig. 2). Here, the conformity reduces almost one order of magnitude at $r \sim 1 h^{-1}$ Mpc and a factor of three at $r \sim 3 h^{-1}$ Mpc in the case ‘PrimNotAC’ compared with the case ‘PrimAll’ for low-mass primary galaxies in the $SAG_{\beta 1.3}$ model.

The modelling of the physical processes that affect the baryonic components implemented in the ILLUSTRISTNG300 hydrodynamical simulation differs from the treatment included in the semi-analytic model from

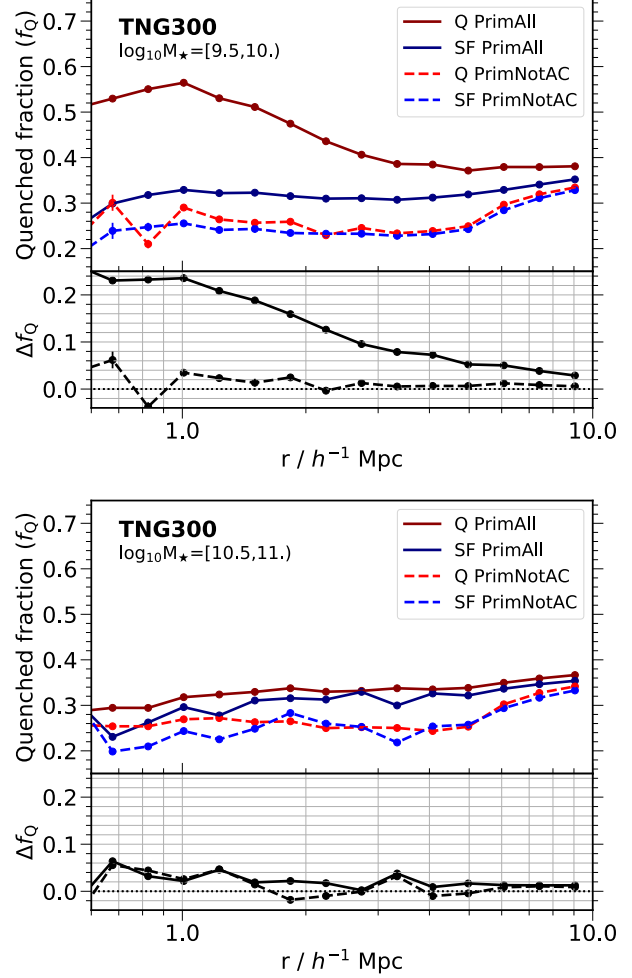


Figure 5. Similar to Fig. 2 but for primary galaxies at fixed stellar mass in the ILLUSTRISTNG300 model (from top to bottom: $10^{9.5} \leq M_{\star}/h^{-1} M_{\odot} < 10^{10}$ and $10^{10.5} \leq M_{\star}/h^{-1} M_{\odot} < 10^{11}$).

which the galaxy catalogues MD_SAG and $SAG_{\beta 1.3}$ are built. Furthermore, the number of synthetic galaxies in ILLUSTRISTNG300 is smaller compared with the SAG catalogues due to the different volume sizes of each simulation. Therefore, the results obtained from ILLUSTRISTNG300 are shown in bigger stellar-mass ranges. The case with *all* the central galaxies, ‘PrimAll’, is shown in Fig. 5 as solid lines. For the lowest stellar mass bin $10^{9.5} \leq M_{\star}/h^{-1} M_{\odot} < 10^{10}$ (top panels), there is evident two-halo conformity out to $r \sim 5 h^{-1}$ Mpc. The difference in the mean quenched fractions of neighbours around low-mass quenched and low-mass star-forming primary galaxies is $\Delta f_Q \sim 0.24$ at $r \sim 1 h^{-1}$ Mpc and it reduces to $\Delta f_Q \lesssim 0.05$ at distances $r \gtrsim 5 h^{-1}$ Mpc from the primary galaxies (black solid line in the sub-panel). In contrast, we do not observe a particular correlation with sSFR between the more massive primary galaxies of $10^{10.5} \leq M_{\star}/h^{-1} M_{\odot} \leq 10^{11}$ and their neighbouring galaxies (bottom panels), where the difference is typically $\Delta f_Q \lesssim 0.04$ at distances $\gtrsim 1 h^{-1}$ Mpc from the intermediate-mass primary galaxies (black solid line in the sub-panel).

Figure 5 also shows the mean quenched fractions of neighbours in the case ‘PrimNotAC’ (dashed lines). As in

the SAMs, the two-halo conformity is very small or absent in this case. For the lowest M_* bin, $10^{9.5} \leq M_*/h^{-1} M_\odot < 10^{10}$, the difference in the mean quenched fractions of neighbours around quenched and star-forming primary galaxies in the case ‘PrimNotAC’ is typical $\Delta f_Q < 0.04$ at distances larger than $1 h^{-1}$ Mpc from the low-mass primary galaxies (black dashed line in the sub-panel). A similar result is obtained for the other massive bin (bottom panels), which resembles the small conformity signal of the fiducial case ‘PrimAll’ in this bin. Therefore, it is a robust result that the conformity measured at few Mpc scales is mainly driven by low-mass central galaxies in the vicinity of groups and clusters because it is independent of the specific model.

In Appendix A, we show the two-halo conformity using the $g-r$ colour. The differences in the mean red fractions in the cases ‘PrimAll’ and ‘PrimNotAC’ are qualitatively very similar to the respective differences in the mean quenched fractions. Therefore, our results are consistent either using sSFR or galaxy colour.

5 DISCUSSION

5.1 Two-halo conformity signal after removing central galaxies

We have shown in Sect. 4 that the conformity signal at few Mpc decreases drastically when the central galaxies in the vicinity of groups and clusters with $M_{200c} \geq 10^{13} h^{-1} M_\odot$ are removed from the primary sample (‘PrimNotAC’). We explore how this signal depends on the halo mass threshold to exclude nearby central galaxies from the primary sample. Fig. 6 shows the mean quenched fractions of neighbours as functions of the distance from low-mass primary galaxies in the ILLUSTRISTNG300 simulation after removing from the primary sample the central galaxies in the vicinity of haloes of different masses. The top panel shows the results for haloes more massive than $10^{13} h^{-1} M_\odot$, i.e. the lines show the same values as the dashed lines in the top panel of Fig. 5. The middle and bottom panels of Fig. 6 show the results obtained when we remove central galaxies in the vicinity of haloes more massive than $10^{13.5}$ and $10^{14} h^{-1} M_\odot$, respectively. The two-halo conformity increases as the halo mass threshold of the systems increases, but the signal at distances $\gtrsim 1 h^{-1}$ Mpc is always smaller than that for the case with *all* the central galaxies in the primary sample (‘PrimAll’ sample; solid lines in the top panel of Fig. 5). The importance of this result is that the two-halo conformity is not produced in the outskirts of galaxy clusters only; we also need to consider the environmental effects in the vicinity of galaxy groups as smaller as $10^{13} h^{-1} M_\odot$ on low-mass central galaxies to largely explain the conformity measured at distances of a few Mpc from the primary galaxies. We note we obtain the same results from the MD_SAG and SAG $_{\beta 1.3}$ catalogues.

We test if the results shown in Sect. 4 are robust or are just an artefact of removing galaxies. For this exercise, we did 50 realizations of removing randomly quenched and star-forming central galaxies from the primary sample in the ILLUSTRISTNG300 simulation. The number of quenched and star-forming central galaxies removed randomly is similar to the case of removing quenched and star-forming central

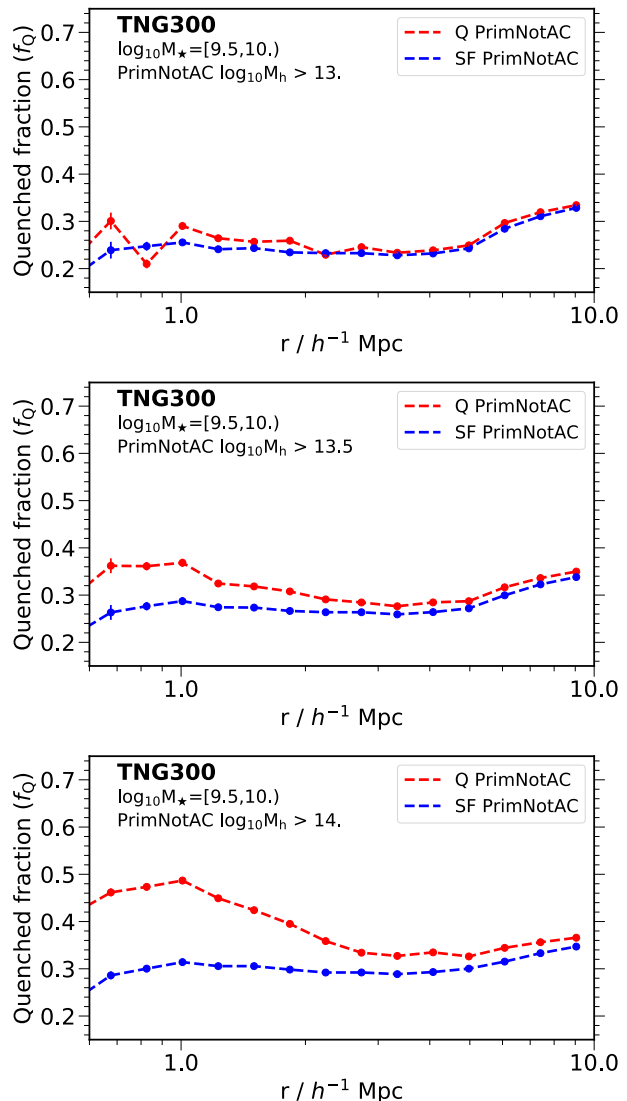


Figure 6. Mean quenched fractions of neighbouring galaxies as functions of the distance from the primary galaxies with stellar masses in the range $10^{9.5} \leq M_*/h^{-1} M_\odot < 10^{10}$ after removing from the primary sample the central galaxies in the vicinity of haloes more massive than $10^{13} h^{-1} M_\odot$ (top), $10^{13.5} h^{-1} M_\odot$ (middle), and $10^{14} h^{-1} M_\odot$ (bottom) in the ILLUSTRISTNG300 simulation. The red and blue dashed lines represent the values for quenched and star-forming primary galaxies, respectively.

galaxies of the same stellar mass in the vicinity of haloes more massive than $10^{13} h^{-1} M_\odot$, ‘PrimNotAC’. Fig. 7 shows the mean quenched fractions of neighbouring galaxies out to $\sim 10 h^{-1}$ Mpc from low-mass primary galaxies ($10^{9.5} \leq M_*/h^{-1} M_\odot < 10^{10}$) for these realizations as solid lines. The results are different than the case ‘PrimNotAC’ shown in dashed lines, but they are similar compared with ‘PrimAll’ (see the solid lines in the top main panel of Fig. 5), i.e., the fiducial conformity signal in the sample ‘PrimAll’ remains after randomly removing central galaxies from the primary sample. This result supports our claim that most of the galactic conformity measured out to scales of a few Mpc is produced by low-mass central galaxies located near large groups and clusters of galaxies.

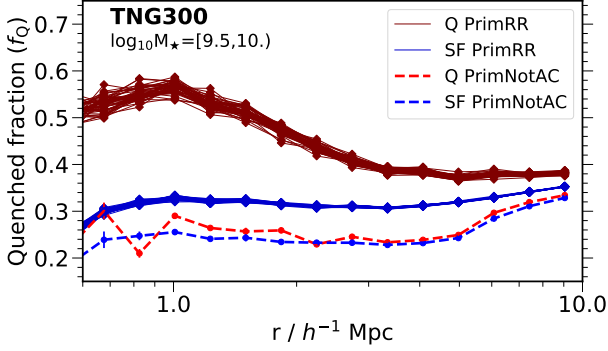


Figure 7. Similar to the top main panel of Fig. 5, where the dashed lines correspond to the ‘PrimNotAC’ sample, but we include 50 realizations of randomly removed quenched and star-forming central galaxies from the ‘PrimAll’ sample in the ILLUSTRIS-TNG300 simulation (maroon and medium blue diamonds, respectively, connected with solid lines).

We also tested with the MD_SAG catalogue that removing central galaxies randomly from the primary sample does not modify the quenched fractions of neighbours at distances of a few Mpc from the primary galaxies in ‘PrimAll’. Therefore, the results shown in the previous section are not an artefact of a spurious emergence of trends due to removing, by chance, a highly biased subset of galaxies. The results from both SAMs and the hydrodynamic simulation are consistent, indicating that most of the galactic conformity measured at few Mpc scales is produced by low-mass central galaxies in the vicinity of large groups and clusters.

5.2 Two-halo conformity signal after varying the vicinity radius

We have considered a radius out to $5 h^{-1}$ Mpc as the scale of influence of massive systems of $M_{200c} \geq 10^{13} h^{-1} M_{\odot}$, which corresponds to a large-scale environment beyond the virial radius of haloes. Here, we test if the previous results are robust after varying this radius out to which we remove the central galaxies from the primary sample.

We test different vicinity radii starting from $1 h^{-1}$ Mpc. We remove from the primary sample the central galaxies inside the vicinity radius of massive systems of $M_{200c} \geq 10^{13} h^{-1} M_{\odot}$ and estimate the mean quenched fractions of neighbouring galaxies around the (remaining) primary galaxies at fixed halo mass. The results for primary galaxies in host dark matter haloes of $10^{11.6} \leq M_{200c}/h^{-1} M_{\odot} < 10^{11.8}$ are shown in Fig. 8. We chose this halo mass range because the fiducial case ‘PrimAll’ shows an evident two-halo conformity signal (see top panel of Fig. 3). The difference in the mean quenched fractions of neighbouring galaxies, i.e., the conformity signal $\Delta f_Q(r)$, typically decreases as the vicinity radius increases. For example, at a distance of $r \sim 3 h^{-1}$ Mpc from the primary galaxies, the conformity signal $\Delta f_Q(3)$ is nearly the same as for the case ‘PrimAll’ (black solid line) and the case of removing from the primary sample the central galaxies in the vicinity of haloes more massive than $10^{13} h^{-1} M_{\odot}$ within 1 and $3 h^{-1}$ Mpc, with $\Delta f_Q(3) \sim 0.06$. The conformity signal reduces down to $\Delta f_Q(3) \sim 0.04$ for the case of removing from the primary sample the central galaxies in the

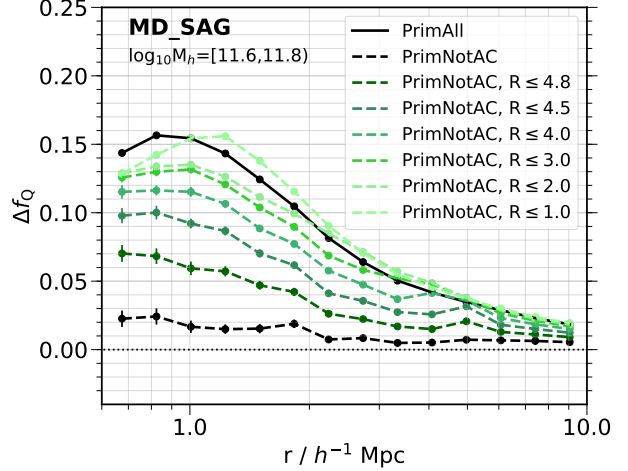


Figure 8. Similar to top sub-panel of Fig. 3, but we include the cases of removing from the primary sample the central galaxies in the vicinity of haloes more massive than $10^{13} h^{-1} M_{\odot}$ out to 1, 2, 3, 4, 4.5, and $4.8 h^{-1}$ Mpc (coloured dashed lines according to the legend).

vicinity of relatively massive haloes within $4 h^{-1}$ Mpc. The conformity signal is $\Delta f_Q(3) \lesssim 0.03$ after removing from the primary sample the central galaxies in the vicinity of haloes more massive than $10^{13} h^{-1} M_{\odot}$ within 4.5 and $5 h^{-1}$ Mpc.

Therefore, the conformity signal at few Mpc scales depends on the vicinity radius around relatively massive haloes. This result can be explained as a combination of the radial influence of haloes that decreases with the cluster-centric radius (e.g., Wetzel, Tinker & Conroy 2012) and that the exact vicinity radius depends on the mass, i.e., it is smaller for less massive groups and larger for more massive clusters (e.g., Bahé et al. 2013). The choice of a relatively large vicinity radius of $5 h^{-1}$ Mpc as the scale of the environmental influence of massive systems on nearby central galaxies is probably considering most of the relevant scales in which this effect has been acting. Zinger et al. (2018) find the star formation quenching via ‘starvation’ can occur in the outskirts of simulated galaxy clusters because their hot X-ray emitting intracluster medium can extend out to ~ 2 – 3 virial radii, which corresponds to median scales of 4–6 Mpc in their sample of clusters, in agreement with our scale of $5 h^{-1}$ Mpc. Similarly, Ayromlou et al. (2021) find the quenched fraction of galaxies in the vicinity of groups and clusters is higher than in the field out to ~ 2 – 3 virial radii using a SAM. We have tested that $\Delta f_Q(r)$ values at distances $r \gtrsim 1 h^{-1}$ Mpc from the primary galaxies are similar for vicinity radii between 5 and $7 h^{-1}$ Mpc, indicating that the environmental influence of massive systems on low-mass central galaxies would not reach scales much more extensive than $5 h^{-1}$ Mpc in our galaxy catalogues. An exploratory analysis in which the vicinity radius varies with the halo mass or other halo properties of the groups and clusters will be presented elsewhere.

5.3 Central galaxies around overdensities

We have tested results from the ‘PrimNotAC’ sample, built by removing central galaxies in the vicinity of groups and clusters from the primary sample. We have considered the halo mass to identify the central galaxies around massive systems. Observationally, it is not easy to infer the halo mass because one has to rely on group finder methods that may contain systematics in the halo mass estimation (e.g., Calderon, Berlind & Sinha 2018; Tinker 2020).

Here, we explore an alternative approach of using dense environments (overdensities) instead of massive haloes. Overdense systems have the advantage that they can be more easily identified in observations depending on the environmental definition. We use the Σ_N parameter, which is a simple estimator to measure the galaxy environment in observations (e.g., Dressler 1980; Aguerri, Méndez-Abreu & Corsini 2009; Domínguez et al. 2002; Nigoche-Netro et al. 2019), with the definition given in Nigoche-Netro et al. (2019), i.e., $\Sigma_N = N/(\pi d_N^2)$, where d_N is the (real-space) distance to the N th nearest neighbouring galaxy. We choose $N = 5$ to measure Σ_5 for each central galaxy using all the galaxies above $7 \times 10^8 h^{-1} M_\odot$ in the $SAG_{\beta 1.3}$ galaxy catalogue.

For consistency with the exercise of Sec. 4 of using the most massive systems, we rank Σ_5 and select the systems with $\log_{10}(\Sigma_5/h^2 \text{ Mpc}^{-2}) \geq 0.856$ as proxies of the overdensities of interest. With this cut, the number of selected overdensities equals the number of haloes with masses $M_{200c} \geq 10^{13} h^{-1} M_\odot$ in $SAG_{\beta 1.3}$. Like in the sample ‘PrimNotAC’, we remove from the primary sample the central galaxies around overdensities (AOD) out to $5 h^{-1}$ Mpc; we refer to this sample as ‘PrimNotAOD’. The results of the conformity for the ‘PrimNotAOD’ sample are shown in Fig. 9 as dashed-dotted lines. They are different to the results obtained from the low-mass sample ‘PrimNotAC’ (also shown in this figure as dashed lines) at distances $r \lesssim 2 h^{-1}$ Mpc from the primary galaxies. The conformity signal is $\Delta f_Q \sim 0.14$ and 0.04 at scales of 1 and $2 h^{-1}$ Mpc, respectively, when the low-mass central galaxies in the vicinity of overdensities are not considered in the primary sample, while $\Delta f_Q \lesssim 0.02$ at scales $\gtrsim 1 h^{-1}$ Mpc for the ‘PrimNotAC’ sample. Both cases are comparable for scales $r \gtrsim 2 h^{-1}$ Mpc, but the former always shows a slightly larger conformity signal than the latter. These results suggest that the environment around groups and clusters, defined by their halo mass, better characterizes conformity at a few Mpc than the environment around overdensities.

We also explore another definition of density environment. Instead of counting galaxies, we count subhaloes in the ILLUSTRISTNG300 simulation, following the approach described in Artale et al. (2018), also implemented in Favole et al. (2022). We use this environmental definition because it is an independent method for selecting overdensities, taking advantage of previously probed in this hydrodynamical cosmological simulation. In this method, we count subhaloes with total mass above $10^{9.5} h^{-1} M_\odot$ within a sphere of radius $3 h^{-1}$ Mpc, centred in dark matter haloes, divided by the volume of the sphere. Unlike Artale et al. (2018), we also include the subhaloes that belong to the same host halo in which the sphere is centred. The calculation is done by adopting periodic boundary conditions and is normalized by

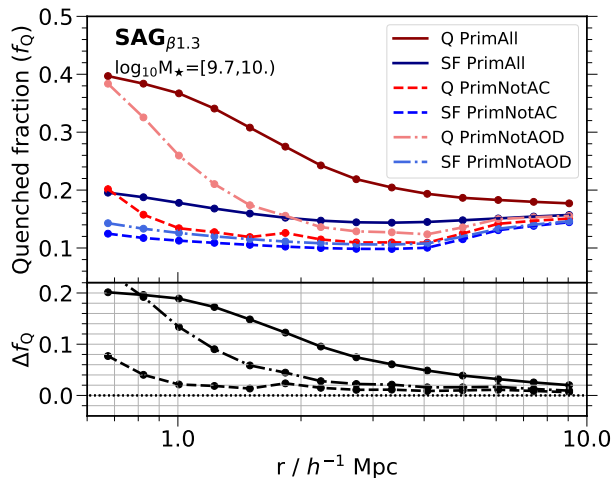


Figure 9. Same as top panel in Fig. 4, but including the ‘PrimNotAOD’ sample based on the Σ_5 environmental estimator. The dashed-dotted lines show the mean quenched fractions after removing from the primary sample the central galaxies in the vicinity of the densest systems in the $SAG_{\beta 1.3}$ catalogue (light coral and royal blue lines for quenched and star-forming primary galaxies, respectively, in the main panels).

the number density of subhaloes in the box with the same mass cut.

We rank the systems using the environmental definition above to identify the highest densities as the overdensity regions of interest. For consistency, the number of the most overdense systems is the same as the number of haloes with $M_{200c} \geq 10^{13} h^{-1} M_\odot$ in ILLUSTRISTNG300. We then remove from the primary sample the central galaxies around these overdensities out to $5 h^{-1}$ Mpc, which we refer again to as the sample ‘PrimNotAOD’. The mean quenched fractions of neighbours for this case are shown in Fig. 10 (dotted lines). The conformity signal is $\Delta f_Q \sim 0.08$ and 0.04 at scales of 1 and $2 h^{-1}$ Mpc, respectively, in the primary sample ‘PrimNotAOD’. These values are smaller than the case with the fiducial sample ‘PrimAll’ (solid lines) with $\Delta f_Q \sim 0.24$ and 0.14 at scales of 1 and $2 h^{-1}$ Mpc. The sample ‘PrimNotAC’ (dashed lines) shows the smallest conformity signal at scales of $\sim 1 h^{-1}$ Mpc with $\Delta f_Q \lesssim 0.04$, but the signals between the cases ‘PrimNotAOD’ and ‘PrimNotAC’ are comparable from scales $r \gtrsim 3 h^{-1}$ Mpc. Again, these results suggest that it is better to characterize the systems that affect nearby low-mass central galaxies, responsible for the two-halo conformity, by the halo mass than the overdensities.

5.4 Why is there a correlation between central galaxies in the vicinity of groups and clusters and neighbouring galaxies?

In this paper, we have demonstrated an excess of correlation between quenched (red), low-mass central galaxies located in the vicinity of galaxy groups and galaxy clusters and quenched (red) neighbouring galaxies out to distances of $r \sim 3 h^{-1}$ Mpc. The two-halo conformity signal Δf_Q (Δf_r) reduces to $\lesssim 0.02$ when these low-mass central galax-

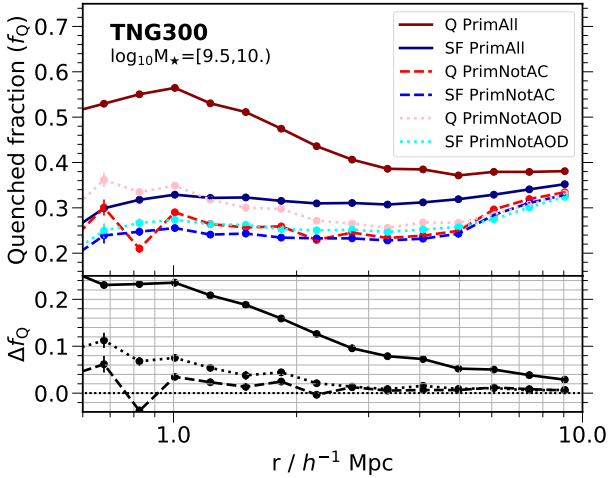


Figure 10. Same as Fig. 9, but for primary galaxies in the stellar mass range $10^{9.5} \leq M_*/h^{-1} M_\odot < 10^{10}$ in the ILLUSTRISTNG300 simulation. In this case, results using an over-density estimator computed on scales of $3 h^{-1}$ Mpc are included (dotted lines, see Sect. 5.3 for details).

ies are not considered in the primary sample. This correlation mainly explains the two-halo conformity found in cosmological simulations and, probably, in observations. Why does this correlation exist?

Here, we make a simple test on checking the distance of quenched and star-forming central galaxies to the nearest massive halo with $M_{200c} \geq 10^{13} h^{-1} M_\odot$ in MD_SAG catalogue. For low-mass central galaxies with $10^{9.7} \leq M_*/h^{-1} M_\odot < 10^{10}$, the median distance is $1.3 h^{-1}$ Mpc for quenched central galaxies, whereas it is $6.2 h^{-1}$ Mpc for star-forming central galaxies. Therefore, quenched low-mass central galaxies are typically much closer to massive haloes than star-forming central galaxies of the same mass (by a factor of ~ 5). For intermediate central galaxies with $10^{10.3} \leq M_*/h^{-1} M_\odot < 10^{10.5}$, the median distances to the nearest massive halo are similar between quenched and star-forming central galaxies (5.4 and $6.1 h^{-1}$ Mpc, respectively), which suggests both populations tend to reside in similar large-scale environments relatively far from the influence of other massive haloes. For more massive central galaxies with $10^{10.5} \leq M_*/h^{-1} M_\odot < 10^{10.7}$, the median distances to the nearest massive halo are $5.5 h^{-1}$ Mpc for quenched centrals and $6.2 h^{-1}$ Mpc for star-forming centrals. These distances are very similar to those in the previous stellar mass bin. The combination of dominant internal processes in more massive galaxies (see Introduction) and the large separation from massive groups and clusters can explain why the two-halo conformity signal is small ($\Delta f_Q \lesssim 0.02$) for central galaxies at intermediate masses and, also, for massive central galaxies.

The median distances of the star-forming central galaxies to the nearest massive halo are remarkably similar between the three stellar-mass ranges. On average, these galaxies continue their expected growth because they are far enough from the influence of massive systems. In contrast, the median distance of low-mass quenched central galaxies to the nearest massive halo is notoriously smaller compared

to those of more massive quenched central galaxies. Our results agree with other works that show the environmental effects are not locked within the virial radius only; they can extend further and affect nearby low-mass galaxies (e.g. Wetzel, Tinker & Conroy 2012; Bahé et al. 2013; Zinger et al. 2018; Ayromlou et al. 2021). The two-halo conformity represents the environmental influence of relatively massive systems out to few Mpc scales.

It is not the scope of this paper to explore those environmental effects, which will be addressed elsewhere, but we can mention some of them studied in the literature. Bahé et al. (2013) find that ram-pressure stripping exerted by the intracluster medium of simulated galaxy groups and clusters, which can be present beyond the virial radius of these systems (e.g. Zinger et al. 2018), can remove the hot gas content of low-mass galaxies ($M_* < 10^{10} M_\odot$) out to ~ 5 virial radii from the groups and clusters in the GIMIC cosmological hydrodynamic simulations. This ram-pressure stripping is much stronger for low-mass galaxies in filaments around clusters. Zinger et al. (2018) applied analytic models in simulated cluster systems and found that the ram-pressure stripping occurring in the outskirts of galaxy clusters may remove the satellite gas halo, but not the cold gas from the galaxy. Ayromlou et al. (2021) show that central galaxies can lose their hot gas via ram-pressure stripping in dense environments before infalling into a more massive halo using a novel version of the L-GALAXIES SAM. This gas stripping is stronger for low-mass central galaxies near massive haloes. Arthur et al. (2019) find a causal link between the instantaneous ram pressure and the gas content of infalling haloes and subhaloes out to ~ 1.5 – 2 virial radii from massive galaxy clusters in resimulated clusters of the THREETHUNDRED project. We note that, in the SAG models, the ram-pressure stripping formalism is only implemented on satellite galaxies within the virial radius of host haloes. This mechanism is not implemented on central galaxies in the outskirts of galaxy groups or clusters.

Any conformity signal obtained from the SAG models in scales involving disconnected halo merger trees should be strictly driven by the different mass growth histories of the dark matter haloes because they depend on the environment. Indirect effects like backsplash galaxies give an alternative explanation. Bahé et al. (2013) find that they have a significant contribution to the systematic depletion of cold gas out to ~ 2 – 3 virial radii from simulated groups and clusters. However, these authors find that this indirect environmental effect is important for galaxies with $M_* > 10^{10} M_\odot$. On the other hand, it has been shown that relatively massive haloes could disrupt the expected growth of near smaller objects and, therefore, affect their properties (e.g. Wang, Mo & Jing 2007; Dalal et al. 2008; Hahn et al. 2009; Salcedo et al. 2018; Mansfield & Kravtsov 2020), which in turn may affect the properties of the central galaxies hosted by these disrupted haloes (e.g. Lacerna & Padilla 2011). Behroozi et al. (2014) find that the smooth accretion of mass of infalling haloes stops at median clustercentric distances of ~ 1.8 virial radii of the final host halo at $z = 0$. Therefore, a feasible effect acting on the quenched, low-mass central galaxies is that the amount of gas accreted by their host dark matter haloes is strongly limited due to the stoppage in the growth of the host haloes produced by the nearby mas-

sive systems. Without gas replenishment, star formation in these low-mass central galaxies is halted.

The correlation between central galaxies in the vicinity of groups and clusters and neighbouring galaxies is because the environment around these massive systems has probably affected the expected growth of nearby haloes and, consequently, of the central galaxies hosted by them. The nearby truncated, low-mass central galaxies are typically quenched and exhibit red colours, similar to satellite galaxies inside the virial radius of massive systems.

6 CONCLUSIONS

We have studied the environment around groups and clusters of galaxies with halo mass $M_{200c} \geq 10^{13} h^{-1} M_{\odot}$ using two galaxy catalogues generated from different versions of the semi-analytic model SAG applied to the MDPL2 cosmological simulation (MD_SAG and SAG $_{\beta 1.3}$ catalogues), and the ILLUSTRISTNG300 cosmological hydrodynamical simulation. Low-mass central galaxies in the vicinity of these massive systems out to $5 h^{-1}$ Mpc are preferentially quenched compared to other central galaxies at fixed stellar mass or fixed host halo mass at $z \sim 0$ in all these cosmological simulations. We find consistently in all the galaxy catalogues that these low-mass central galaxies, especially those in the vicinity of galaxy groups, mostly produces the two-halo galactic conformity measured at large separations of several Mpc between the low-mass central galaxy and neighbouring galaxies in adjacent haloes.

In summary, we measure the mean quenched fractions of neighbouring galaxies as functions of the real space distance from quenched primary galaxies and star-forming primary galaxies. The primary samples correspond to central galaxies in the simulations. The galactic conformity signal for a given distance, $\Delta f_{\text{Q}}(r)$, is measured as the difference between these mean quenched fractions at fixed mass of the primary galaxies. For the fiducial sample ‘PrimAll’, the conformity is important for low-mass primary galaxies ($M_{\star} \leq 10^{10} h^{-1} M_{\odot}$), with $\Delta f_{\text{Q}} \sim 0.15$, ~ 0.19 , and ~ 0.24 at $r \sim 1 h^{-1}$ Mpc in the MD_SAG, SAG $_{\beta 1.3}$, and the ILLUSTRISTNG300 simulation, respectively. The conformity signal declines to Δf_{Q} values lower than 0.02 at distances larger than $7 h^{-1}$ Mpc from the low-mass primary galaxies in these simulations (Figs. 2, 4, and 5). The conformity signal is significantly reduced when the central galaxies in the vicinity of groups and clusters are removed from the primary sample (‘PrimNotAC’) with $\Delta f_{\text{Q}} \lesssim 0.02$ for scales $r \gtrsim 1 h^{-1}$ Mpc in both SAMs (Figs. 2 and 4), and $\Delta f_{\text{Q}} \lesssim 0.02$ at $r \gtrsim 1.5 h^{-1}$ Mpc in ILLUSTRISTNG300 (Fig. 5). The low-mass central galaxies in the vicinity of low-mass groups are responsible for the majority of the conformity signal (Fig. 6).

The trends with the conformity signal remain for primary galaxies at fixed halo mass. For primary galaxies in low-mass host haloes of $10^{11.4} \leq M_{200c}/h^{-1} M_{\odot} < 10^{11.6}$ in the MD_SAG catalogue, $\Delta f_{\text{Q}} \sim 0.16$ at $r \sim 1 h^{-1}$ Mpc in the sample ‘PrimAll’, and it reduces to $\Delta f_{\text{Q}} \sim 0.02$ at scales larger than $7 h^{-1}$ Mpc. However, Δf_{Q} is $\lesssim 0.02$ at distances $r \gtrsim 1 h^{-1}$ Mpc from the primary galaxies in the sample ‘PrimNotAC’ (Fig. 3).

We tested that the results in the sample ‘PrimNotAC’ are not an artefact of removing galaxies in the primary sam-

ple. Removing central galaxies randomly from the primary sample does not modify the quenched fractions of neighbours at distances of a few Mpc from the primary galaxies in ‘PrimAll’ (Fig. 7). The conformity signal at few Mpc scales depends on the vicinity radius around relatively massive haloes in which we remove central galaxies, though (Fig. 8), but we tested that this influence on low-mass central galaxies does not reach scales much more extensive than $5 h^{-1}$ Mpc.

We also explored the effects in central galaxies around overdensities (‘PrimNotAOD’) instead of the case around massive haloes. By using two definitions for selecting the densest systems, the case ‘PrimNotAOD’ is comparable to the case ‘PrimNotAC’ for scales $r \gtrsim 2-3 h^{-1}$ Mpc, but the environment around groups and clusters defined by their halo mass better characterizes the two-halo conformity than the environment around overdensities at $r \gtrsim 1 h^{-1}$ Mpc, in general (Figs. 9 and 10).

The quenched, low-mass central galaxies are much closer to massive haloes than star-forming central galaxies of the same mass (by a factor of ~ 5). Future works will be needed to determine if the host haloes of the quenched, low-mass central galaxies have been disrupted by the overwhelming presence of nearby massive haloes, which in turn may affect the expected star formation of these low-mass central galaxies.

ACKNOWLEDGEMENTS

The authors acknowledge the kind support of the computing team at IATE. The authors thank the anonymous referee for the revision that helped improve the presentation of this paper. FR, ALO and ANR thanks the support by *Agencia Nacional de Promoción Científica y Tecnológica, Consejo Nacional de Investigaciones Científicas y Técnicas* (CONICET, Argentina), and *Secretaría de Ciencia y Tecnología de la Universidad Nacional de Córdoba* (SeCyT-UNC, Argentina). ADMD thanks Fondecyt for financial support through the Fondecyt Regular 2021 grant 1210612. SAC acknowledges funding from *Consejo Nacional de Investigaciones Científicas y Técnicas* (CONICET, PIP-0387), *Agencia Nacional de Promoción de la Investigación, el Desarrollo Tecnológico y la Innovación* (Agencia I+D+i, PICT-2018-3743), and *Universidad Nacional de La Plata* (G11-150), Argentina. MCA acknowledges financial support from the Austrian National Science Foundation through FWF stand-alone grant P31154-N27. CVM acknowledges support from ANID/FONDECYT through grant 3200918, and he also acknowledges support from the Max Planck Society through a Partner Group grant. The authors gratefully acknowledge the Gauss Centre for Supercomputing e.V. (www.gauss-centre.eu) and the Partnership for Advanced Supercomputing in Europe (PRACE, www.prace-ri.eu) for funding the MultiDark simulation project by providing computing time on the GCS Supercomputer SuperMUC at Leibniz Supercomputing Centre (LRZ, www.lrz.de).

DATA AVAILABILITY

The data underlying this article is available as follows. The MD_SAG galaxy catalogue is publicly available at the Cos-

moSim database <http://www.cosmosim.org/>. The $SAG_{\beta 1.3}$ galaxy catalogue will be shared on reasonable request to the corresponding author. The ILLUSTRISTNG300 simulation is publicly available at the TNG website <https://www.tng-project.org/>.

REFERENCES

- Aguerri J. A. L., Méndez-Abreu J., Corsini E. M., 2009, *A&A*, 495, 491
- Alam S., Peacock J. A., Kraljic K., Ross A. J., Comparat J., 2020, *MNRAS*, 497, 581
- Alpaslan M. et al., 2015, *MNRAS*, 451, 3249
- Aragon-Salamanca A., Ellis R. S., Couch W. J., Carter D., 1993, *MNRAS*, 262, 764
- Argudo-Fernández M., Lacerna I., Duarte Puertas S., 2018, *A&A*, 620, A113
- Artale M. C., Zehavi I., Contreras S., Norberg P., 2018, *MNRAS*, 480, 3978
- Arthur J. et al., 2019, *MNRAS*, 484, 3968
- Ayromlou M., Kauffmann G., Yates R. M., Nelson D., White S. D. M., 2021, *MNRAS*, 505, 492
- Bahé Y. M. et al., 2017, *MNRAS*, 470, 4186
- Bahé Y. M., McCarthy I. G., Balogh M. L., Font A. S., 2013, *MNRAS*, 430, 3017
- Behroozi P. S., Wechsler R. H., Lu Y., Hahn O., Busha M. T., Klypin A., Primack J. R., 2014, *ApJ*, 787, 156
- Behroozi P. S., Wechsler R. H., Wu H.-Y., 2013, *ApJ*, 762, 109
- Behroozi P. S., Wechsler R. H., Wu H.-Y., Busha M. T., Klypin A. A., Primack J. R., 2013, *ApJ*, 763, 18
- Benítez-Llambay A., Navarro J. F., Abadi M. G., Gottlöber S., Yepes G., Hoffman Y., Steinmetz M., 2013, *ApJL*, 763, L41
- Berti A. M., Coil A. L., Behroozi P. S., Eisenstein D. J., Bray A. D., Cool R. J., Moustakas J., 2017, *ApJ*, 834, 87
- Blanton M. R., Moustakas J., 2009, *ARA&A*, 47, 159
- Bluck A. F. L., Mendel J. T., Ellison S. L., Moreno J., Simard L., Patton D. R., Starkenburg E., 2014, *MNRAS*, 441, 599
- Bluck A. F. L. et al., 2016, *MNRAS*, 462, 2559
- Bose S., Eisenstein D. J., Hernquist L., Pillepich A., Nelson D., Marinacci F., Springel V., Vogelsberger M., 2019, *MNRAS*, 490, 5693
- Bower R. G., Benson A. J., Malbon R., Helly J. C., Frenk C. S., Baugh C. M., Cole S., Lacey C. G., 2006, *MNRAS*, 370, 645
- Bray A. D. et al., 2016, *MNRAS*, 455, 185
- Brown T. et al., 2017, *MNRAS*, 466, 1275
- Calderon V. F., Berlind A. A., Sinha M., 2018, *MNRAS*, 480, 2031
- Campbell D., van den Bosch F. C., Hearin A., Padmanabhan N., Berlind A., Mo H. J., Tinker J., Yang X., 2015, *MNRAS*, 452, 444
- Collacchioni F., Cora S. A., Lagos C. D. P., Vega-Martínez C. A., 2018, *MNRAS*, 481, 954
- Contreras S., Angulo R. E., Zennaro M., 2021, *MNRAS*, 508, 175
- Cora S. A., 2006, *MNRAS*, 368, 1540
- Cora S. A. et al., 2018, *MNRAS*, 479, 2
- Cortese L., Catinella B., Boissier S., Boselli A., Heinis S., 2011, *MNRAS*, 415, 1797
- Cybulski R., Yun M. S., Fazio G. G., Gutermuth R. A., 2014, *MNRAS*, 439, 3564
- Dalal N., White M., Bond J. R., Shirokov A., 2008, *ApJ*, 687, 12
- Davis M., Efstathiou G., Frenk C. S., White S. D. M., 1985, *ApJ*, 292, 371
- Delfino F. M., Scóccola C. G., Cora S. A., Vega-Martínez C. A., Gargiulo I. D., 2022, *MNRAS*, 510, 2900
- Dolag K., Borgani S., Murante G., Springel V., 2009, *MNRAS*, 399, 497
- Domínguez M. J., Zandivarez A. A., Martínez H. J., Merchán M. E., Muriel H., Lambas D. G., 2002, *MNRAS*, 335, 825
- Donnari M., Pillepich A., Nelson D., Marinacci F., Vogelsberger M., Hernquist L., 2021, *MNRAS*, 506, 4760
- Donnari M. et al., 2019, *MNRAS*, 485, 4817
- Dressler A., 1980, *ApJ*, 236, 351
- Duckworth C., Tojeiro R., Kraljic K., Sgró M. A., Wild V., Weijmans A.-M., Lacerna I., Drory N., 2019, *MNRAS*, 483, 172
- Favole G., Montero-Dorta A. D., Artale M. C., Contreras S., Zehavi I., Xu X., 2022, *MNRAS*, 509, 1614
- Gargiulo I. D. et al., 2015, *MNRAS*, 446, 3820
- Garling C. T., Peter A. H. G., Kochanek C. S., Sand D. J., Crnojević D., 2020, *MNRAS*, 492, 1713
- Gavazzi G., Consolandi G., Gutierrez M. L., Boselli A., Yoshida M., 2018, *A&A*, 618, A130
- Genel S. et al., 2014, *MNRAS*, 445, 175
- Gill S. P. D., Knebe A., Gibson B. K., 2005, *MNRAS*, 356, 1327
- Giovanelli R., Haynes M. P., 1985, *AJ*, 90, 2445
- Goddard D. et al., 2017, *MNRAS*, 465, 688
- Gunn J. E., Gott J. R. I., 1972, *ApJ*, 176, 1
- Guo K. et al., 2019, *ApJ*, 870, 19
- Hadzhiyska B., Bose S., Eisenstein D., Hernquist L., Spergel D. N., 2020, *MNRAS*, 493, 5506
- Haggar R., Gray M. E., Pearce F. R., Knebe A., Cui W., Mostoghiu R., Yepes G., 2020, *MNRAS*, 492, 6074
- Hahn O., Porciani C., Dekel A., Carollo C. M., 2009, *MNRAS*, 398, 1742
- Hearin A. P., Behroozi P. S., van den Bosch F. C., 2016, *MNRAS*, 461, 2135
- Hearin A. P., Watson D. F., van den Bosch F. C., 2015, *MNRAS*, 452, 1958
- Hirschmann M., De Lucia G., Iovino A., Cucciati O., 2013, *MNRAS*, 433, 1479
- Kauffmann G., 2015, *MNRAS*, 454, 1840
- Kauffmann G., Li C., Zhang W., Weinmann S., 2013, *MNRAS*, 430, 1447
- Klypin A., Yepes G., Gottlöber S., Prada F., Heß S., 2016, *MNRAS*, 457, 4340
- Knebe A. et al., 2018, *MNRAS*, 474, 5206
- Knobel C., Lilly S. J., Woo J., Kovač K., 2015, *ApJ*, 800, 24
- Kraljic K. et al., 2019, *MNRAS*, 483, 3227
- Kuutma T., Tamm A., Tempel E., 2017, *A&A*, 600, L6
- Lacerna I., Contreras S., González R. E., Padilla N., Gonzalez-Perez V., 2018, *MNRAS*, 475, 1177
- Lacerna I., Padilla N., 2011, *MNRAS*, 412, 1283

- Lagos C. D. P., Cora S. A., Padilla N. D., 2008, MNRAS, 388, 587
- Larson R. B., Tinsley B. M., Caldwell C. N., 1980, ApJ, 237, 692
- Lee H.-R., Lee J. H., Jeong H., Park B.-G., 2016, ApJ, 823, 73
- Li L.-C., Qin B., Wang J., Wang J., Wang Y.-G., 2021, Research in Astronomy and Astrophysics, 21, 032
- Lin L. et al., 2010, ApJ, 718, 1158
- Lin L. et al., 2019, ApJ, 872, 50
- Maier C., Haines C. P., Ziegler B. L., 2022, A&A, 658, A190
- Mansfield P., Kravtsov A. V., 2020, MNRAS, 493, 4763
- Marinacci F. et al., 2018, MNRAS, 480, 5113
- McCarthy I. G., Frenk C. S., Font A. S., Lacey C. G., Bower R. G., Mitchell N. L., Balogh M. L., Theuns T., 2008, MNRAS, 383, 593
- Montero-Dorta A. D. et al., 2020, MNRAS, 496, 1182
- Montero-Dorta A. D., Chaves-Montero J., Artale M. C., Favole G., 2021, MNRAS, 508, 940
- Moore B., Katz N., Lake G., Dressler A., Oemler A., 1996, Nature, 379, 613
- Moore B., Lake G., Katz N., 1998, ApJ, 495, 139
- Muñoz Arancibia A. M., Navarrete F. P., Padilla N. D., Cora S. A., Gawiser E., Kurczynski P., Ruiz A. N., 2015, MNRAS, 446, 2291
- Muriel H., Coenda V., 2014, A&A, 564, A85
- Naiman J. P. et al., 2018, MNRAS, 477, 1206
- Navarro J. F., Frenk C. S., White S. D. M., 1997, ApJ, 490, 493
- Nelson D. et al., 2018, MNRAS, 475, 624
- Nelson D. et al., 2019, Computational Astrophysics and Cosmology, 6, 2
- Nigoche-Netro A., Ramos-Larios G., Lagos P., de la Fuente E., Ruelas-Mayorga A., Mendez-Abreu J., Kemp S. N., Diaz R. J., 2019, MNRAS, 488, 1320
- Norberg P., Baugh C. M., Gaztañaga E., Croton D. J., 2009, MNRAS, 396, 19
- Orsi Á., Padilla N., Groves B., Cora S., Tecce T., Gargiulo I., Ruiz A., 2014, MNRAS, 443, 799
- Otter J. A., Masters K. L., Simmons B., Lintott C. J., 2020, MNRAS, 492, 2722
- Pallero D., Gómez F. A., Padilla N. D., Torres-Flores S., Demarco R., Cerulo P., Olave-Rojas D., 2019, MNRAS, 488, 847
- Pandey B., Sarkar S., 2020, MNRAS, 498, 6069
- Paranjape A., Kovač K., Hartley W. G., Pahwa I., 2015, MNRAS, 454, 3030
- Peng Y., Maiolino R., Cochrane R., 2015, Nature, 521, 192
- Peng Y.-j. et al., 2010, ApJ, 721, 193
- Phillips J. I., Wheeler C., Boylan-Kolchin M., Bullock J. S., Cooper M. C., Tollerud E. J., 2014, MNRAS, 437, 1930
- Pillepich A. et al., 2018a, MNRAS, 475, 648
- Pillepich A. et al., 2018b, MNRAS, 473, 4077
- Pimbblet K. A., 2011, MNRAS, 411, 2637
- Planck Collaboration et al., 2014, A&A, 571, A16
- Planck Collaboration et al., 2016, A&A, 594, A13
- Rafieferantsoa M., Davé R., 2018, MNRAS, 475, 955
- Roberts I. D., Parker L. C., Brown T., Joshi G. D., Hlavacek-Larrondo J., Wadsley J., 2019, ApJ, 873, 42
- Rodríguez F., Montero-Dorta A. D., Angulo R. E., Artale M. C., Merchán M., 2021, MNRAS, 505, 3192
- Ruiz A. N. et al., 2015, ApJ, 801, 139
- Salcedo A. N., Maller A. H., Berlind A. A., Sinha M., McBride C. K., Behroozi P. S., Wechsler R. H., Weinberg D. H., 2018, MNRAS, 475, 4411
- Schaefer A. L. et al., 2019, MNRAS, 483, 2851
- Sin L. P. T., Lilly S. J., Henriques B. M. B., 2017, MNRAS, 471, 1192
- Sin L. P. T., Lilly S. J., Henriques B. M. B., 2019, MNRAS, 488, 234
- Solanes J. M., Manrique A., García-Gómez C., González-Casado G., Giovanelli R., Haynes M. P., 2001, ApJ, 548, 97
- Spindler A. et al., 2018, MNRAS, 476, 580
- Springel V., 2010, MNRAS, 401, 791
- Springel V. et al., 2018, MNRAS, 475, 676
- Springel V., White S. D. M., Tormen G., Kauffmann G., 2001a, MNRAS, 328, 726
- Springel V., White S. D. M., Tormen G., Kauffmann G., 2001b, MNRAS, 328, 726
- Sun S., Guo Q., Wang L., Lacey C. G., Wang J., Gao L., Pan J., 2018, MNRAS, 477, 3136
- Tecce T. E., Cora S. A., Tissera P. B., Abadi M. G., Lagos C. D. P., 2010, MNRAS, 408, 2008
- Tinker J. L., 2020, arXiv e-prints, arXiv:2007.12200
- Tinker J. L., Hahn C., Mao Y.-Y., Wetzel A. R., Conroy C., 2018, MNRAS, 477, 935
- Tremmel M. et al., 2019, MNRAS, 483, 3336
- Treyer M. et al., 2018, MNRAS, 477, 2684
- Vega-Martínez C. A., Gómez F. A., Cora S. A., Hough T., 2022, MNRAS, 509, 701
- Vogelsberger M. et al., 2014a, Nature, 509, 177
- Vogelsberger M. et al., 2014b, MNRAS, 444, 1518
- Wang H. Y., Mo H. J., Jing Y. P., 2007, MNRAS, 375, 633
- Weinberger R. et al., 2017, MNRAS, 465, 3291
- Weinmann S. M., van den Bosch F. C., Yang X., Mo H. J., 2006, MNRAS, 366, 2
- Wetzel A. R., Tinker J. L., Conroy C., 2012, MNRAS, 424, 232
- Xie L., De Lucia G., Hirschmann M., Fontanot F., 2020, MNRAS, 498, 4327
- Zehavi I. et al., 2002, ApJ, 571, 172
- Zhang Y., Yang X., Guo H., 2021, MNRAS, 507, 5320
- Zheng Z. et al., 2019, ApJ, 873, 63
- Zheng Z. et al., 2017, MNRAS, 465, 4572
- Zinger E., Dekel A., Kravtsov A. V., Nagai D., 2018, MNRAS, 475, 3654
- Zu Y., Mandelbaum R., 2018, MNRAS, 476, 1637

APPENDIX A: CONFORMITY WITH COLOUR

We explore the two-halo conformity trends using the $g - r$ colour. Fig. A1 shows the mean red fractions of neighbouring galaxies as functions of the distance from the primary galaxies in two stellar-mass bins in the MD_SAG galaxy catalogue. The solid lines correspond to the case ‘PrimAll’. The correlation in the red colour between neighbours and primary galaxies at distances of a few Mpc is much stronger for low-mass primaries ($10^{9.7} \leq M_*/h^{-1} M_\odot < 10^{10}$) compared with primaries at intermediate masses ($10^{10.3} \leq M_*/h^{-1} M_\odot < 10^{10.5}$). The differences in the mean red fractions of neighbours around red and blue primary galaxies, Δf_r , are shown

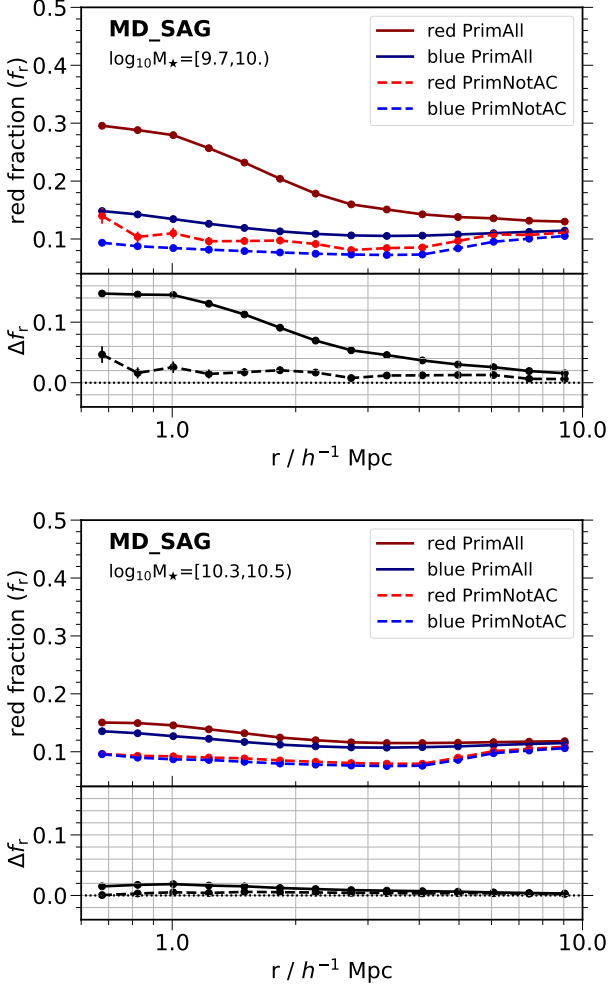


Figure A1. Similar as Fig. 2 but using $g - r$ colour instead of sSFR.

with black solid lines in the sub-panels. For the low-mass primaries, Δf_r is as big as ~ 0.14 at $\sim 1 h^{-1}$ Mpc, it decreases to ~ 0.05 at $\sim 3 h^{-1}$ Mpc, and it is smaller than 0.02 at distances $\gtrsim 7 h^{-1}$ Mpc. For primary galaxies of intermediate masses, Δf_r is typical $\lesssim 0.02$ at all the scales. These results are both qualitatively and quantitatively very similar to the difference in the mean quenched fractions (black solid lines in Fig. 2). Therefore, there is a clear correlation between neighbouring galaxies and low-mass primary galaxies in both the colour and sSFR out to distances of a few Mpc.

The case ‘PrimNotAC’, in which we remove from the primary sample the central galaxies in the vicinity of groups and clusters, is shown as dotted lines in Fig. A1. The difference in the mean red fractions of the case ‘PrimNotAC’ is typical $\Delta f_r \lesssim 0.03$ at distances $\gtrsim 1 h^{-1}$ Mpc from low-mass primary galaxies, and it is smaller for the intermediate-mass primary galaxies. For the low-mass primary galaxies, Δf_r decreases a factor of 3–4 at 2–3 h^{-1} Mpc in ‘PrimNotAC’ compared with ‘PrimAll’. The overall behaviour of the mean red fractions in the case ‘PrimNotAC’ is qualitatively very similar to the same case of the mean quenched fractions (dotted lines in Fig. 2). Therefore, the observed correlation

in both colour and sSFR between low-mass central galaxies and neighbour galaxies at distances of a few Mpc is mainly driven by the central galaxies located in the outskirts of groups and clusters of galaxies.

Taking into account the remarkable similarity between the results obtained from the MD_SAG and SAG $_{\beta 1.3}$ models, and the ILLUSTRISTNG300 simulation when considering the sSFR, it is reasonable to expect that the same trend is maintained in the SAG $_{\beta 1.3}$ and ILLUSTRISTNG300 galaxy catalogues when considering colours. Indeed, this is the case, but we do not show such analysis here.